TECHNICAL REPORT RD-SS-92-11

THE EQUIVALENT FLAT NOSE DIAMETER OF HEMISPHERICAL NOSE CYLINDRICAL PROJECTILES FOR IMPACT INDUCED DETONATION OF ENERGETIC MATERIALS

James P. Billingsley
James M. Oliver
Systems Simulation and Development Directorate
Research, Development, and Engineering Center

December 1992

U.S. ARMY MISSILE COMMAND
Redstone Arsenal, Alabama 35898-5000

Approved for Public Release; Distribution is unlimited.

DESTRUCTION NOTICE

FOR CLASSIFIED DOCUMENTS, FOLLOW THE PROCEDURES IN DoD 5200.22-M, INDUSTRIAL SECURITY MANUAL, SECTION II-19 OR DoD 5200.1-R, INFORMATION SECURITY PROGRAM REGULATION, CHAPTER IX. FOR UNCLASSIFIED, LIMITED DOCUMENTS, DESTROY BY ANY METHOD THAT WILL PREVENT DISCLOSURE OF CONTENTS OR RECONSTRUCTION OF THE DOCUMENT.

DISCLAIMER

THE FINDINGS IN THIS REPORT ARE NOT TO BE CONSTRUED AS AN OFFICIAL DEPARTMENT OF THE ARMY POSITION UNLESS SO DESIGNATED BY OTHER AUTHORIZED DOCUMENTS.

TRADE NAMES

USE OF TRADE NAMES OR MANUFACTURERS IN THIS REPORT DOES NOT CONSTITUTE AN OFFICIAL ENDORSEMENT OR APPROVAL OF THE USE OF SUCH COMMERCIAL HARDWARE OR SOFTWARE.

UNCLASSIFIED

SECURITY CLASSIFICATION OF THIS PAGE

REPORT DOCUMENTATION PAGE

Form Approved
OMB No. 0704-0188
Exp. Date: Jun 30, 1986

1a. REPORT SECURITY CLASSIFICATION UNCLASSIFIED	1b. RESTRICTIVE MARKINGS
2a. SECURITY CLASSIFICATION AUTHORITY	3. DISTRIBUTION/AVAILABILITY OF REPORT Approved for Public Release; Distribution Unlimited
2b. DECLASSIFICATION/DOWNGRADING SCHEDULE	
4. PERFORMING ORGANIZATION REPORT NUMBER(S) TR–RD–SS–92–11	5. MONITORING ORGANIZATION REPORT NUMBER(S)
6a. NAME OF PERFORMING ORGANIZATION Sys. Sim. and Dev. Dir. Res., Dev., and Eng. Ctr 6b. OFFICE SYMBOL (If applicable) AMSMI–RD–SS	7a. NAME OF MONITORING ORGANIZATION
6c. ADDRESS (City, State, and ZIP Code) Commander, U.S. Army MICOM ATTN: AMSMI–RD–SS Redstone Arsenal, AL 35898–5252	7b. ADDRESS (City, State, and ZIP Code)
8a. NAME OF FUNDING/SPONSORING ORGANIZATION 8b. OFFICE SYMBOL (If applicable)	9 PROCUREMENT INSTRUMENT IDENTIFICATION NUMBER
8c. ADDRESS (City, State, and ZIP Code)	10. SOURCE OF FUNDING NUMBERS PROGRAM ELEMENT NO. / PROJECT NO. / TASK NO. / WORK UNIT ACCESSION NO.

11. TITLE (Include Security Classification)
The Equivalent Flat Nose Diameter of Hemispherical Nose Cylindrical Projectiles for Impact Induced Detonation of Energetic Materials

12. PERSONAL AUTHOR(S)
Billingsley, James P. and Oliver, James M.

13a. TYPE OF REPORT	13b. TIME COVERED	14. DATE OF REPORT (Year, Month, Day)	15. PAGE COUNT
Final	FROM Sept 91 TO Sept 92	December 1992	

16. SUPPLEMENTARY NOTATION

17. COSATI CODES			18. SUBJECT TERMS (Continue on reverse if necessary and identify by block number)	
FIELD	GROUP	SUB-GROUP	Detonation Criteria	PBX–9404
			Impacted Explosives	COMP–B
			Shocked Explosives	Energetic Materials

19. ABSTRACT (Continue on reverse if necessary and identify by block number)

The analysis of explosive detonation via projectile impact is inherently complex because of the many variables which must be considered. One very important variable is the nose or tip shape of the projectile which contacts the bare unprotected planar surface of the energetic material. This report demonstrates that Hemispherical Nose (HN) projectiles (cylindrical, rods, or spheres) are equivalent to a much smaller Flat Nose (FN) surface. This equivalence is suggested by comparison with appropriate theory and a very limited amount of experimental data for two explosives (PBX–9404 and COMP–B).

20. DISTRIBUTION/AVAILABILITY OF ABSTRACT	21. ABSTRACT SECURITY CLASSIFICATION	
☒ UNCLASSIFIED/UNLIMITED ☐ SAME AS RPT. ☐ DTIC USERS	UNCLASSIFIED	
22a. NAME OF RESPONSIBLE INDIVIDUAL Dr. Billingsley, James P.	22b. TELEPHONE (Include Area Code) (205)–876–5210	22c. OFFICE SYMBOL AMSMI–RD–SS–AA

DD FORM 1473, 84 MAR — 83 APR edition may be used until exhausted. All other editions are obsolete.

SECURITY CLASSIFICATION OF THIS PAGE

UNCLASSIFIED

TABLE OF CONTENTS

LIST OF ILLUSTRATIONS

I. INTRODUCTION

Analysis of shock induced explosive detonation via general projectile impact is complicated not only by impact velocity (V_I), projectile material, length, and cross–sectional area requirements but by projectile nose shape as well. The simplest nose shape from an analytical viewpoint is flat (FN) or planar. A conical shape is next in complexity, followed by the hemispherical (HN). Many projectiles while penetrating armor and/or cover plates will erode and acquire essentially a hemispherical profile. Consequently, the hemispherical shape is important from academic and practical considerations.

An earlier analysis of experimental data for impact shock induced detonation via FN cylindrical projectiles is documented in Reference 1. In this work, some simple empirical relations were derived which are functions of the projectile cross–sectional area and known impact shock variables. These relations were introduced to enhance and/or supplement current empirical detonation prediction methodology.

It is the purpose of the present report to demonstrate that for detonation of one explosive (PBX–9404), the HN shape is equivalent to a much smaller FN shape at the same impact velocity (V_I). The demonstration is accomplished by comparing theoretical and experimental information. It is shown that the equivalent flat nose diameter (D_{FNEQ}) of a HN projectile (D_{HN}) is:

$$D_{FNEQ} = \left(\frac{V_I}{U_{SP}}\right) D_{HN} \tag{1}$$

where:

U_{SP} = Shock front velocity in the projectile(steel).

A very limited amount of experimental data was available for the COMP–B explosive. This datum (one point) compares favorably with the above relation when a reasonable extrapolation of FN experimental information is performed. These experimental data are discussed more thoroughly in Section II.

References 2, 3, and 4 also contain analyses of hemispherical nose projectile impact shock induced detonation of explosives. The general emphasis and scope of these documents differ somewhat from that of the present report.

Here, the thrust is to delineate the flat nose equivalent diameter (D_{FNEQ}) of HN shapes. This is important, since when D_{FNEQ} is found from Equation 1, then it can be employed for the diameter, D, in the empirical relations described in Reference 1 for FN projectiles. If equivalence actually exists, then there should be correlation with the FN projectile relations in Reference 1. Two examples of this type of correlation are given for the Held explosive sensitivity parameter, $V_I \sqrt{D}$, and the comparison is satisfactory.

II. EXPERIMENTAL INFORMATION

Reference 1 contains a rather detailed analysis of five sets of experimental impact induced detonation data for five different secondary explosives. These data from diverse sources had been systematically acquired by firing flat faced projectiles with different cross–section area and different velocities (V_I) into flat explosive specimens.

The basic result of these experimental investigations was that the impact velocity (V_I) necessary to cause detonation was highly dependent on the projectile cross–section area dimensions or rod diameter (D_{FN}). Some of these data from Reference 5 for PBX–9404 are shown in Figure 1 (V_I versus D_{FN}). The line shown is the boundary between detonation and no detonation. Detonation occurs for points above the line and does not occur for points below the line. Detonation occurred for the six points illustrated, so the demarcation line shown is conservative (Detonation always occurs for points above the line).

Reference 5 also contains similar experimental information for PBX–9404 subjected to impact by steel cylinders with hemispherical tips. The diameter (D_{HN}) and impact velocity were systematically varied to ascertain the demarcation limits. This information is also shown in Figure 1. Detonation occurs for all the points shown except one, which is denoted by a dark or filled–in symbol. The faired demarcation line goes between the "NO GO" point and the nearby "GO" point and passes through or above the other "GO" points. Thus, it is believed to be conservative.

Reference 6 contains experimental information for the detonation demarcation limits of PBX–9404 and COMP–B when struck by a spherical steel projectile. Only one diameter (1.3 cm) was employed but the striking velocity was varied to define the critical velocity, V_{CR}, for each explosive. Examination of Figure 2 in Reference 6 reveals the following critical velocities where detonation was certain to occur:

Explosive	V_{CR} (Km/sec)
PBX–9404	1.14
COMP–B	1.75

This "GO" point for PBX–9404 is plotted in Figure 1 where it agrees closely with the information from Reference 5 for the hemispherical tipped cylindrical rod projectiles. This is interesting since it illustrates the importance of nose shape as contrasted to the overall shape (rod or sphere). Apparently the length of the sphere (its diameter) is large enough so that reflected tensile stress waves from the rear do not diminish the main compressive pulse magnitude (P_S) before a critical amount of time (T_{CR}) has elapsed. See Reference 1 for additional information concerning for the importance of the compressive shock pulse duration (T_{CR}).

The steel spherical projectile "GO" point for COMP–B is shown in Figure 2. No information for hemispherical tipped cylindrical tipped rod impact induced detonation is available for COMP–B. However, there is information for flat nose cylindrical projectile induced detonation available in Reference 7. Three critical experimentally derived data points (V_I, D_{FN}) from Reference 7 are shown in Figure 2 and this defines the detonation demarcation curve for COMP–B and flat nose cylindrical rod projectiles. Note the extrapolation of this demarcation line to a region of smaller D_{FN} and large V_I. This non–linear extrapolation is considered to be a reasonable representation of the detonation demarcation line in this important region. It was done so

that an "experimental" value of D_{FNEQ} could be graphically estimated as shown in Figure 2 for the single data point of the spherical projectile striking COMP–B.

A similar example for PBX–9404 is illustrated in Figure 1 for one of the HN rod projectiles. For a given V_I which produces detonation, the hemispherical nose diameter (D_{HN}) has to be much larger than the corresponding flat nose equivalent diameter (D_{FNEQ}).

Thus, the hemispherical nose is not as efficient in producing detonation as a flat nose. In other words, a large portion of the HN projectile diameter (D_{HN}) is ineffective so far as impact shock induced detonation is concerned. Only a much smaller portion (D_{FNEQ}) is effective and it can be experimentally ascertained as described above and illustrated in Figures 1 and 2. Experimental values of D_{FNEQ} for the HN and spherical projectiles are given in Table 1.

The appropriate theory is discussed in the following section.

III. EQUIVALENT FLAT NOSE DIAMETER (D_{FNEQ})

The contents of Reference 1 delineate the importance of the projectile flat nose area for impact shock induced detonation. That is, an undisturbed plane or one dimensional shock pressure must act on a critical area (A_{CR}) for a specific amount of time (T_{CR}) or detonation will not occur. Both Moulard's critical area concept and the Walker–Wasley critical energy concept must be satisfied.

Thus, intuitively, it should not seem strange that only a portion of a hemispherical nose area (or diameter) would be effective for shock induced detonation. This would be "almost flat" part of the surface near the projectile centerline.

Reference 8 provides a relatively simple analysis which indicates how much of the hemispherical curved impacted surface would experience essentially an undisturbed or undiminished shock pressure pulse before a release or rarefaction (tensile stress) wave forms and propagates back into the shocked material. The rarefaction relieves the relatively high compressive shock pressure. The time and place of its occurrence influences the duration (T_{CR}) and area (A or A_{CR}) coverage of the undiminished shock pressure, P_S.

First of all in Reference 8, it is shown for a flat faced projectile that the critical angle of yaw is:

$$\phi_{CR} = \text{ARCSIN}\,(V_I / U_{sp}) \qquad (2)$$

The critical yaw angle , ϕ_{CR}, is depicted in Figure 3 which is similar to Figure 10b of Reference 8. For angles less than ϕ_{CR}, the magnitude and duration of the shock pressure are practically the same as an unyawed projectile. For yaw angles greater than ϕ_{CR}, the full Hugoniot shock pressure exists only at the point of contact.

In addition, it is indicated in Reference 8 that Equation 2 also defines the critical angle for the full Hugoniot shock pressure duration and affected area of a curved surface impacting a flat target. This is illustrated in Figure 4 for a hemispherical nose shape. Figure 4 is similar to Figure 11 of Reference 8.

The angle, ϕ, between the flat target surface and the projectile curved surface changes and increases as penetration increases. When ϕ exceeds ϕ_{CR}, a rarefaction (tensile) wave forms at the

projectile surface/target surface edge contact point and propagates back into the shocked region. This reduces the Hugoniot pressure duration and its areal coverage.

In Section II, it was shown how the effective or equivalent diameter (D_{FNEQ}) of HN projectiles was determined from experimental data. Figure 5 illustrates the geometrical relationship between D_{FNEQ} and D_{HN}. They are related to an angle, ϕ_{EQ}, which is:

$$\phi_{EQ} = \text{ARCSIN}\,(D_{FNEQ}/D_{HN}) \tag{3}$$

So far, two angles, ϕ_{CR} and ϕ_{EQ}, have been defined for the hemispherical shape via Equations 2 and 3, respectively. To ascertain whether these angles were equal or related, they were computed and compared as follows.

The angle ϕ_{CR} was computed for all the HN and spherical projectile impact data discussed in Section II. The results are listed in Table 2 and plotted versus V_I in Figure 6. Figure 7 illustrates V_I/U_{SP} plotted versus V_I. See the Appendix for additional information regarding the computation of U_{SP} and P_S. These computations took account of the Hugoniot Elastic Limit (HEL) and 130 KBAR transition point that occurs in iron and mild steel [9 and 10].

The equivalent flat nose diameters (D_{FNEQ}) for each of the HN and spherical projectiles were determined graphically from the experimental data plots as illustrated in Figures 1 and 2. For a given V_I, the shock pressure (P_S) must be the same for both FN and HN or spherical projectiles. When D_{FNEQ} is found, then ϕ_{EQ} is computed via Equation 3. This information is listed in Table 1 and depicted in Figures 6 and 7 as a function of V_I.

The comparative information in Figures 6 and 7 reveals that essentially:

$$\phi_{CR} = \phi_{EQ} \tag{4}$$

or

$$\frac{D_{FNEQ}}{D_{HN}} = \frac{V_I}{U_{SP}} \tag{5}$$

In Figure 8, D_{FNEQ}/D_{HN} is plotted versus V_I/U_{SP} and the comparison is essentially one–to–one. Thus practically, for the limited amount available:

$$D_{FNEQ} = \left(\frac{V_I}{U_{SP}}\right) D_{HN} \tag{1}$$

$$= \text{a function of } V_I$$

Although the magnitudes of ϕ_{CR}, ϕ_{EQ}, or D_{FNEQ}/D_{HN}, V_I/U_{SP} still compare favorably for PBX–9404 at V_I = 1.95 km/sec or V_I/U_{SP} = 0.385 the data trend is different. There is a crossover of ϕ_{EQ} and D_{FNEQ}/D_{HN} from being slightly greater than ϕ_{CR} and V_I/U_{SP}, respectively to being somewhat smaller (Figs. 6, 7, and 8). This may be caused by the projectile material behavior since P_S is greater than 130 Kbars, which is a phase change point and for iron and mild steels.

Note that in Table 2, the second wave shock velocity at the 130 Kbar point was employed in Equation 2 rather than the slower third wave velocity. The results at V_I = 1.70 km/sec may

also be influenced by this projectile material phase change. Some additional experimental data at higher V_I conditions and smaller projectile diameters are needed to more completely define the data trend. Systematic testing with other projectile materials such as tungsten alloys (which are commonly used in severe impact applications) is needed for a variety of important explosives.

It was noted in Section I that if D_{FNEQ} equivalence is a valid concept, then there should be good agreement with various FN projectile data correlation parameters such as the widely used explosive sensitivity parameter ($V_I \sqrt{D}$ = constant) which was first suggested by Dr. Manfred Held in 1968 [11, 12, and 13]. The Held constant differs for different explosives. In Reference 1, Appendix E, this sensitivity parameter is evaluated for PBX–9404 and COMP–B for the same FN projectile data which is shown in Figures 1 and 2, respectively.

The flat nose sensitivity factor, $V_I\sqrt{D}$, for PBX–9404 and COMP–B is tabulated in Reference 1 and is plotted versus V_I in Figures 9 and 10, respectively of the present report. Also shown in these Figures are the results for $V_I \sqrt{D_{FNEQ}}$ for the HN and the spherical projectiles considered in this report. The tabulated values are listed in Tables 2 and 3.

Note that in Tables 3 and 4 D_{FNEQ} is not the experimental value shown in Table 1. D_{FNEQ} is computed via Equation 1, such as could or would be done in an engineering application to predict detonation if experimental data were not available. These $V_I \sqrt{D_{FNEQ}}$ results compare reasonably well with the FN projectile parameter, $V_I\sqrt{D_{FN}}$.

It is believed that the equivalent flat nose diameter concept could also be applied to correlate (via the Held parameter as described above) some of the shaped charge jet/explosive detonation data. However, the jet tip shape can vary a considerable amount [14] so that a complete correlation may not be possible. As time and circumstances permit, an attempt to correlate the shaped charge jet /detonation data via the $V_I \sqrt{D_{FNEQ}}$ parameter will be made.

IV. CONCLUSIONS

A small sample of experimental data have been used to derive what appears to be a valid geometric equivalence relationship suitable for detonation predictive purposes in those cases involving flat nosed and hemispherical projectiles. The HN shape is important from a practical point of view. Many "Sharp–pointed" projectiles have a small hemispherical tip. Also blunt or flat projectiles erode during penetration of armor and/or shields, and the resulting shape is approximately hemispherical. If an energetic material is being shielded, Equation 1 and the Held sensitivity coefficient can be employed in detonation prediction analyses. Also the equivalent flat nosed diameter concept may be applicable to shaped charge jets as mentioned in Section III.

V. RECOMMENDATIONS

The data and analysis reported here suggest that detonation data acquired using impact of Flat nosed projectiles on bare explosives can be used to establish detonation criteria for projectiles of other symmetric shapes. Additional testing such as reported in References 5, 6, and 7 is required to validate the postulated geometric equivalence definition for flat nosed and hemispherical tipped projectiles.

Table 1. Experimental Results for D_{FNEQ} and ϕ_{EQ}

Explosive ~	D_{HN} cm	D_{FNEQ} cm	D_{FNEQ}/D_{HN} ~	ϕ_{EQ} Deg.
PBX–9404	0.4445	0.150	0.3375	19.72
[5]	0.5080	0.175	0.3445	20.15
	0.6300	0.200	0.3175	18.51
	1.1430	0.308	0.2695	15.63
	1.2700	0.330	0.2598	15.06
	1.7780	0.405	0.2278	13.17
PBX–9404 [6]	1.300 (Spherical)	0.320	0.2461	14.25
COMP–B [6]	1.300 (Spherical)	(0.420)*	0.3231	18.85

* See Text, Section II

Table 2. Computed Results for U_{SP} and ϕ_{CR}

Explosive ~	D_{HN} cm	V_I km/sec	U_{SP} km/sec	U_{PP} km/sec	P_S Kbars	U_{SEX} km/sec	U_{PEX} km/sec	V_I/U_{SP} ~	ϕ_{CR} Deg
PBX–9404	0.4445	1.95	5.069*	0.470	166.9	6.120	1.480	0.3847	22.62
[5]	0.5080	1.70	5.069*	0.375	140.0	5.736	1.325	0.3354	19.60
	0.6300	1.53	5.037	0.306	123.7	5.485	1.224	0.3037	17.68
	1.1430	1.21	4.927	0.223	89.0	4.898	0.987	0.2456	14.22
	1.2700	1.16	4.910	0.211	84.0	4.804	0.949	0.2363	13.66
	1.7780	1.04	4.872	0.182	72.4	4.578	0.858	0.2135	12.33
PBX–9404 [6]	1.300 Spherical	1.14	4.900	0.203	82.0	4.773	0.937	0.2326	13.45
COMP–B [6]	1.300 Spherical	1.75	5.062	0.325	129.1	5.33	1.425	0.3457	20.22

*Iron Shock Velocity at 130 Kbar Transition Point

Table 3. The Held Explosive Sensitivity Factor, $V_I\sqrt{D_{FNEQ}}$, for Hemispherical Projectiles Striking PBX–9404

V_I	V_I/U_{SP}	D_{HN}	D_{FNEQ} $(V_I/U_{SP}*D_{HN})$	$\sqrt{D_{FNEQ}}$	$V_I\sqrt{D_{FNEQ}}$	$V_I^2D_{FNEQ}$
mm/μ–sec	~	mm	mm	$mm^{1/2}$	$mm^{3/2}/\mu$–sec	mm^3/μ–sec^2
1.95	0.3847	4.445	1.710	1.308	2.550	6.502
1.70	0.3354	5.080	1.704	1.305	2.219	4.92.4
1.53	0.3037	6.300	1.913	1.383	2.116	4.479
1.21	0.2456	11.430	2.807	1.675	2.027	4.110
1.16	0.2363	12.700	3.001	1.732	2.010	4.038
1.04	0.2135	17.780	3.796	1.948	2.026	4.106
1.14	0.2326	13.00 (spherical projectile)	3.024	1.739	1.982	3.930 spherical

Table 4. The Held Explosive Sensitivity Factor, $V_I\sqrt{D_{FNEQ}}$, for a Spherical Projectile Striking COMP–B

V_I	V_I/U_{SP}	D_S	D_{FNEQ} $(V_I/U_{SP}*D_{HN})$	$\sqrt{D_{FNEQ}}$	$V_I\sqrt{D_{FNEQ}}$	$V_I^2D_{FNEQ}$
mm/μ–sec	~	mm	mm	$mm^{1/2}$	$mm^{3/2}/\mu$–sec	mm^3/μ–sec^2
1.75	0.3457	13.00	4.494	2.120	3.71	13.76

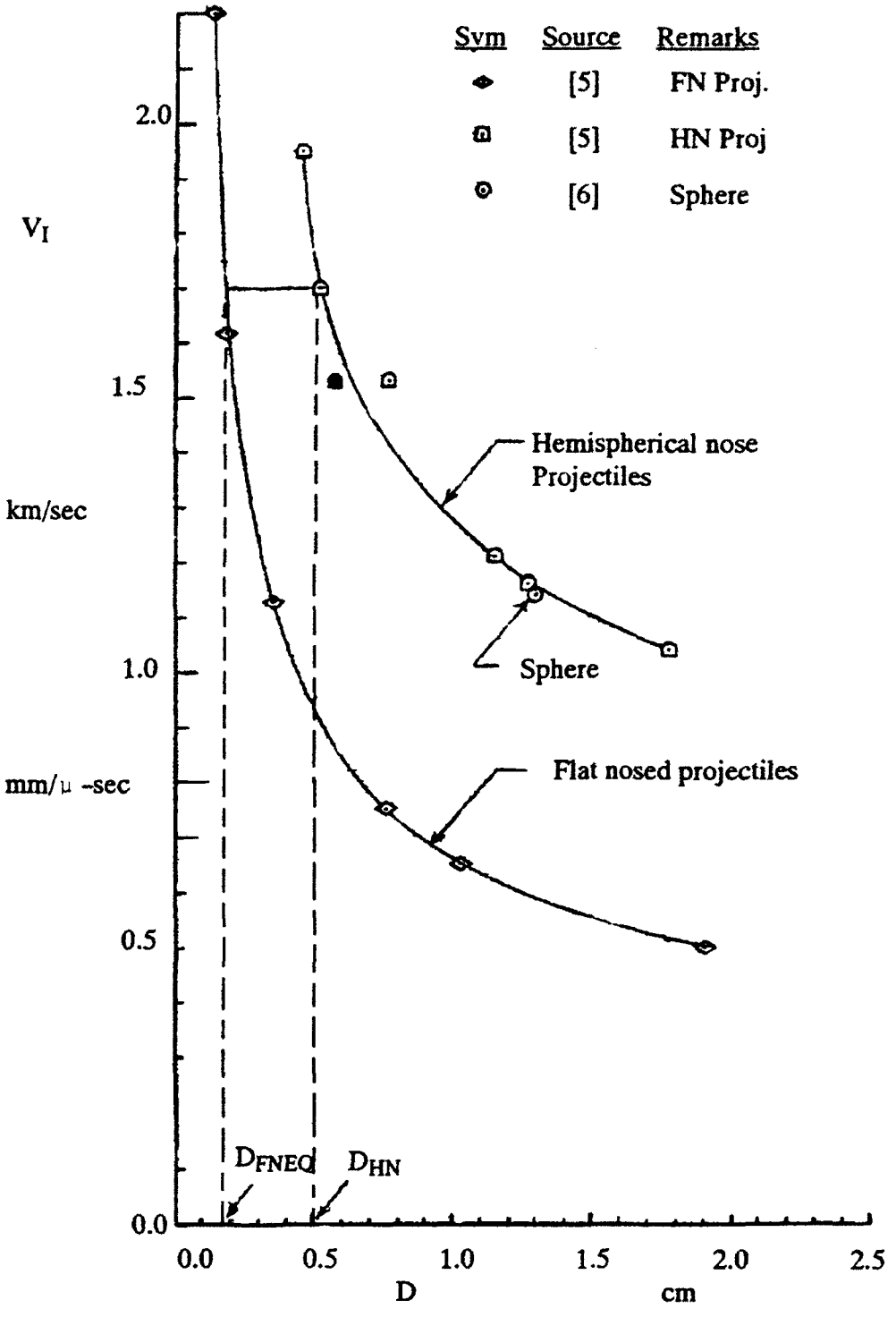

Figure 1. Impact Velocity Required to Detonate PBX–9404 for Different Projectile Diameters

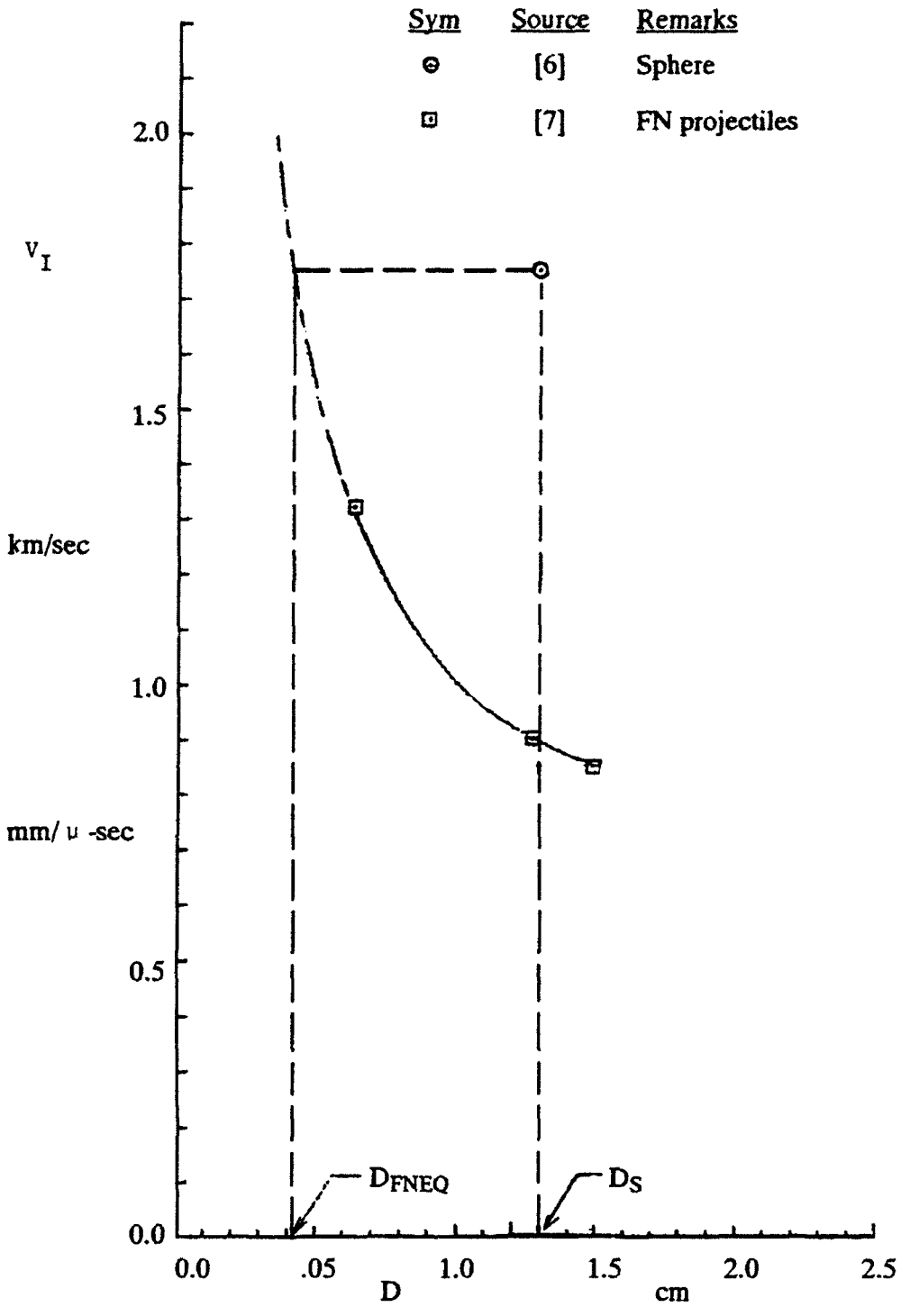

Figure 2. Impact Velocity Required to Detonate COMP–B for Different Projectile Diameters

$$\sin\phi_{CR} = \frac{V_I}{U_{SP}}$$

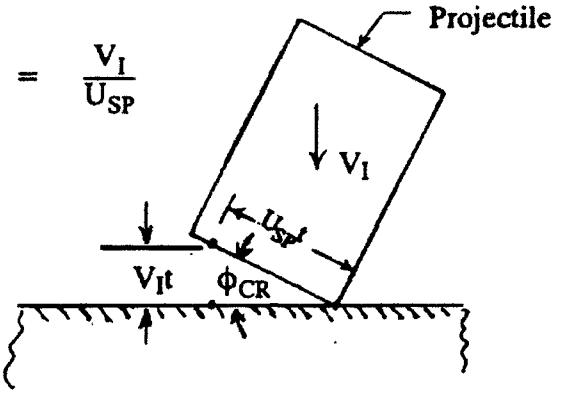

Figure 3. Critical Contact Conditions for a Flat Nose Projectile Impacting a Flat Target

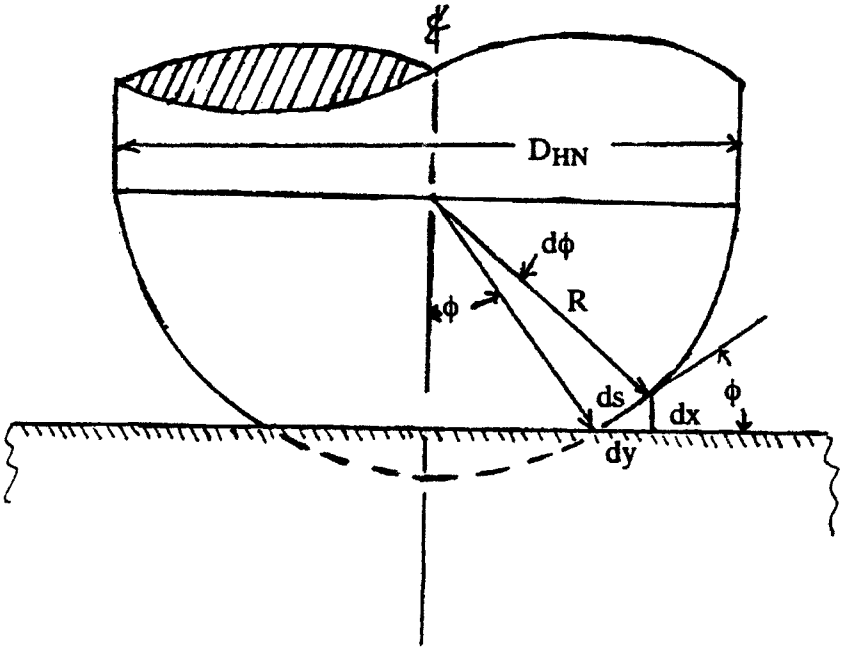

$$U_{SP}\,dt = ds = Rd\phi$$

$$V_I\,dt = dx = ds\sin\phi CR = Rd\phi\sin\phi_{CR}$$

$$\frac{V_I}{U_{SP}} = \frac{dx}{ds} = \frac{Rd\phi}{Rd\phi}\sin\phi_{CR} = \sin\phi_{CR}$$

Figure 4. Critical Contact Conditions for a Hemispherical Nose Projectile Impacting a Flat Target

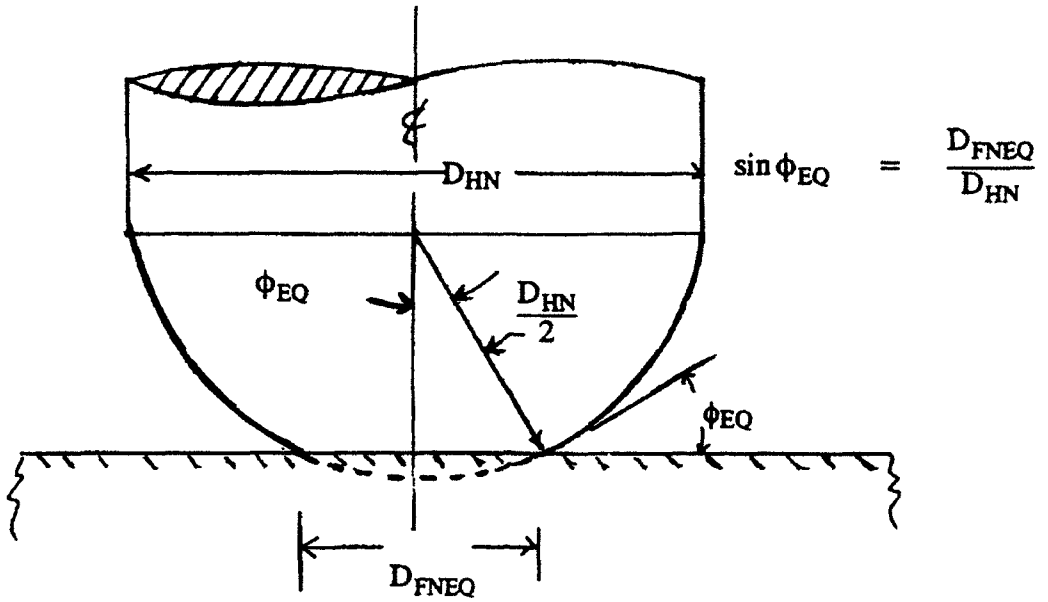

Figure 5. Schematic of Equavalent Flat Nose Diameter (D_{FNEQ}) for Hemispherical Projectiles

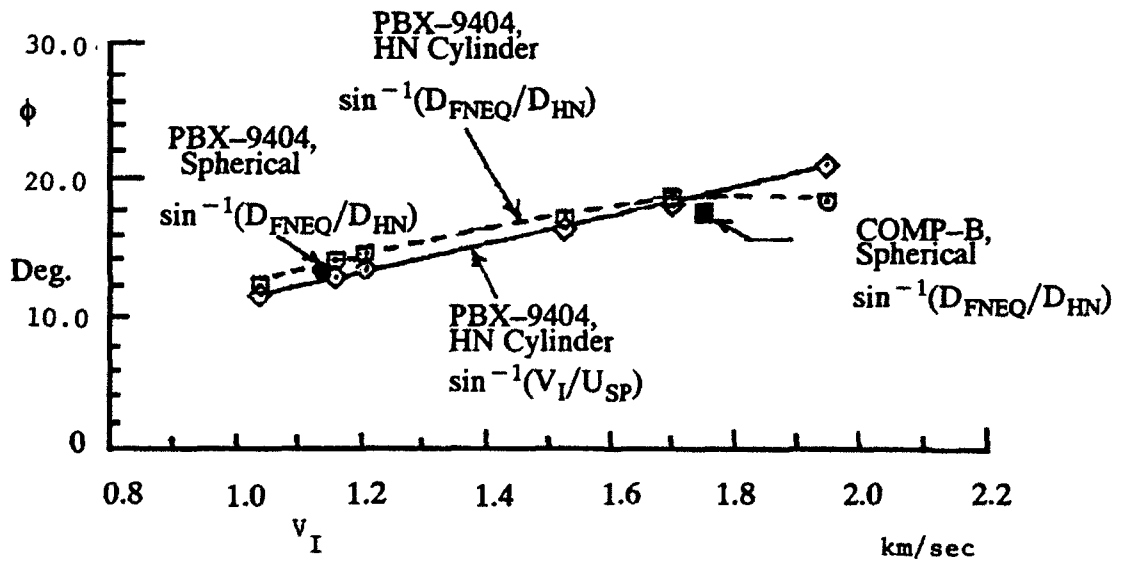

Figure 6. ϕ Versus V_I

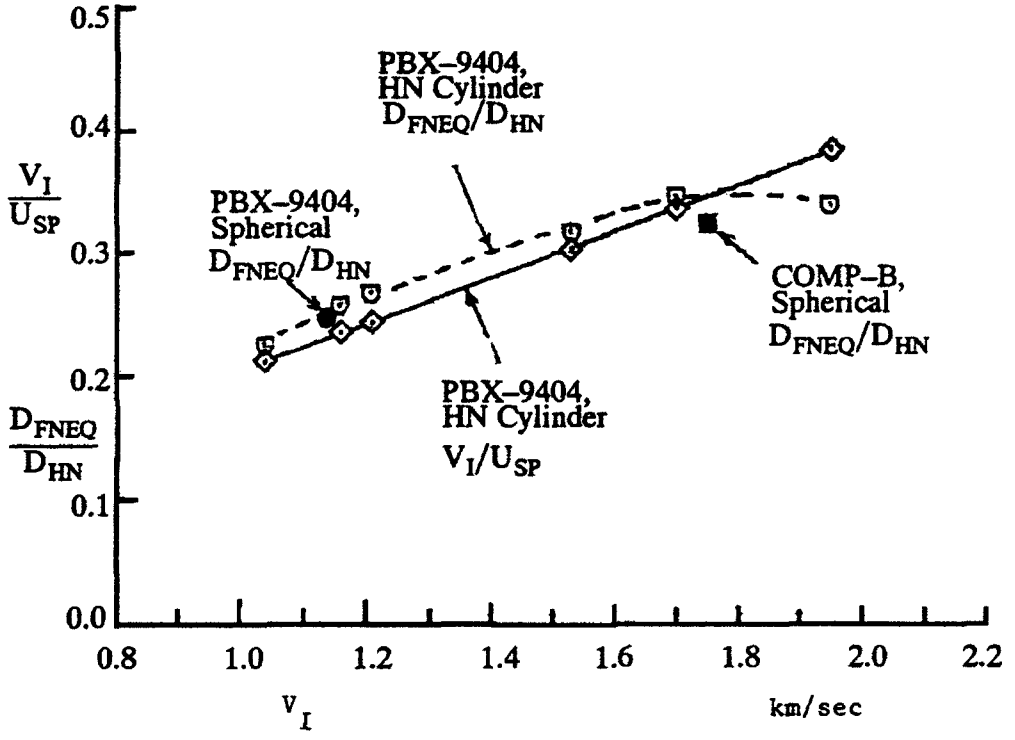

Figure 7. V_I/U_{SP} and D_{FNEQ}/D_{HN} Versus V_I

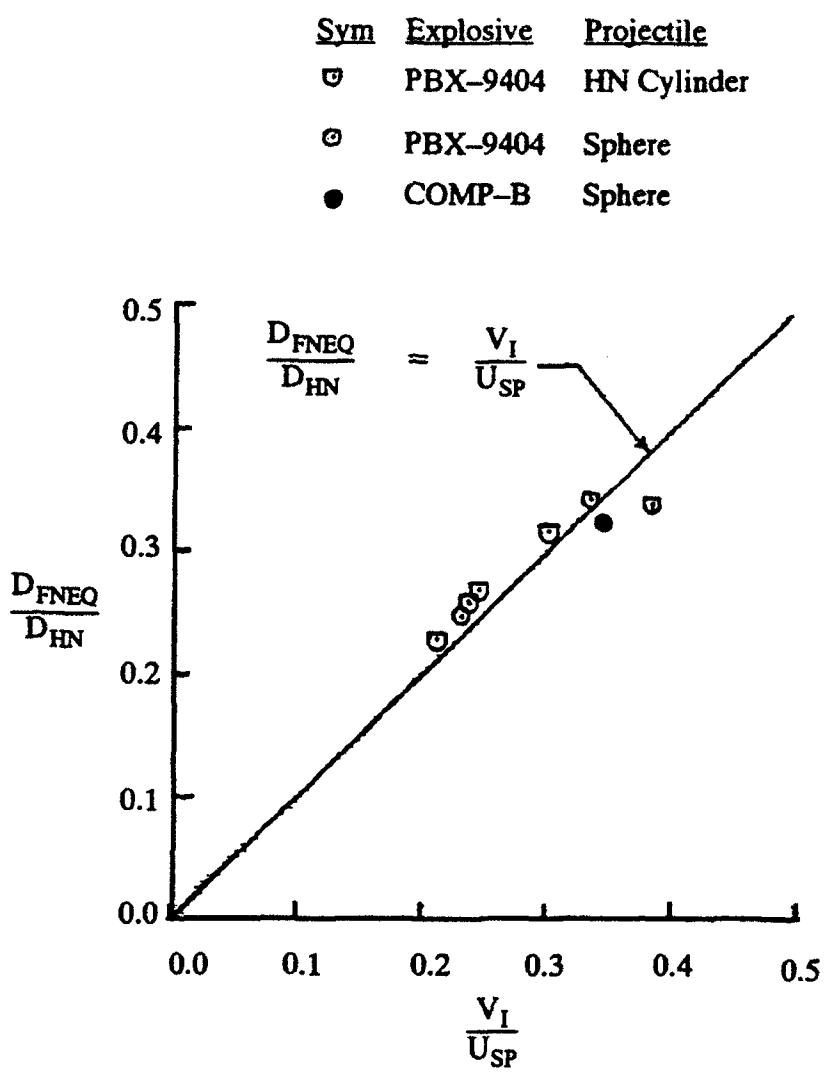

Figure 8. D_{FNEQ}/D_{HN} Versus V_I/U_{SP}

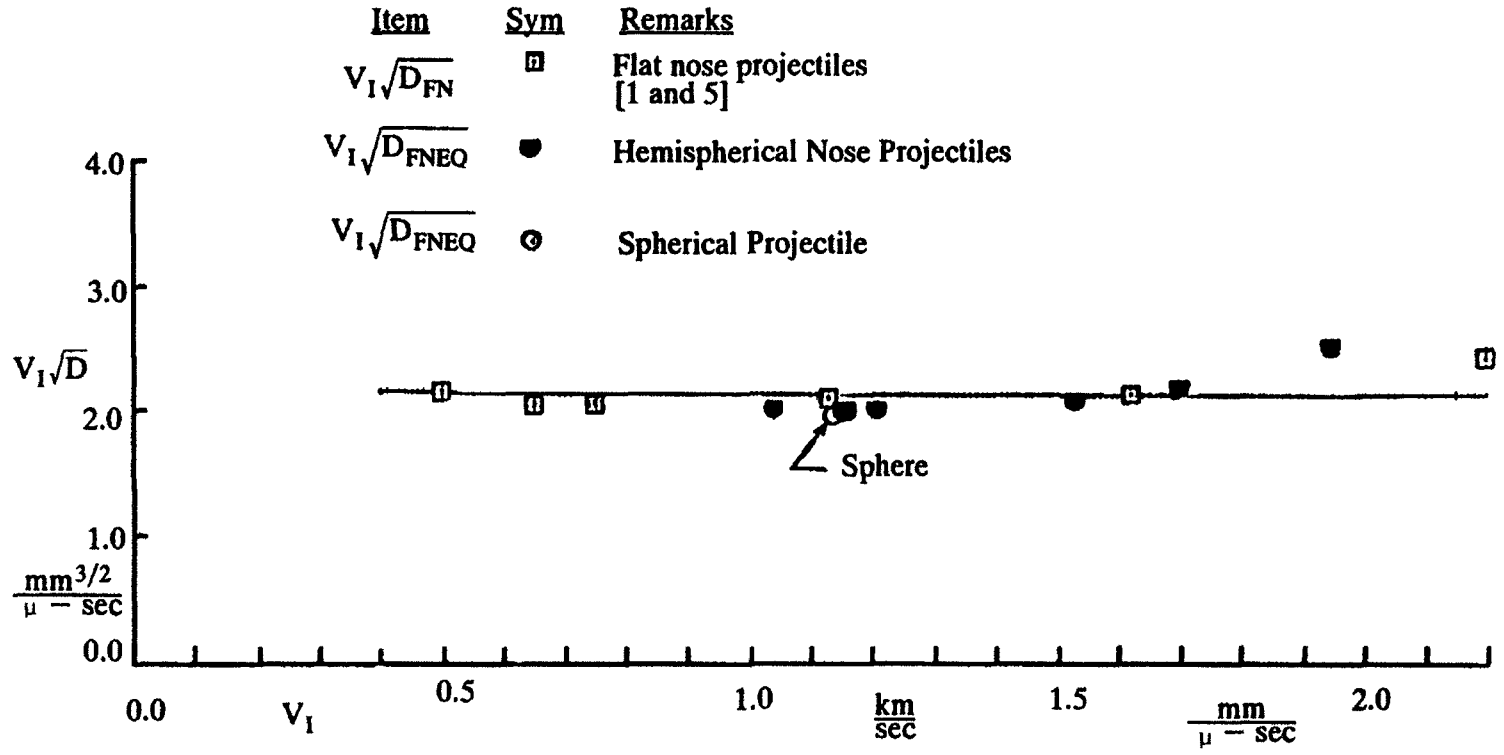

Figure 9. The Held Parameter, $V_I\sqrt{D}$, Versus V_I for PBX–9404

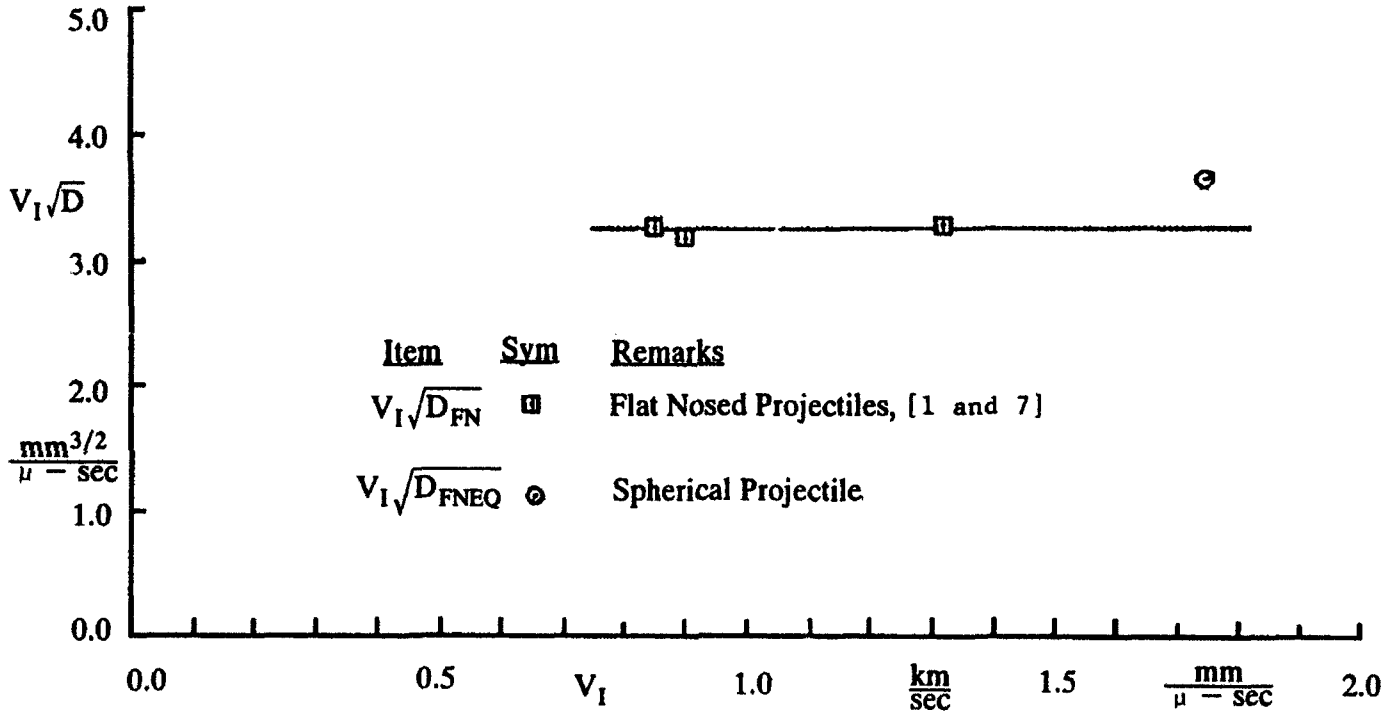

Figure 10. The Held Parameter, $V_I\sqrt{D}$, Versus V_I for COMP–B

REFERENCES

1. Billingsley, J.P. and Adams, C.L.; "Remarks on Certain Aspects of Solid Explosive Detonation via Small Projectile Impact." MICOM TR–RD–SS–88–11, (May 1989), Aeroballistics Analysis Branch, Systems Simulation and Development Directorate, Research Development and Engineering Center, USAMICOM, Redstone Arsenal, AL 35898.
2. Fishburn, Barry D. ; "An Analysis of Impact Ignition of Explosives and the Currently Used Threshold Criteria", TR–ARAED–TR–90029, Nov. 1990 , U. S. Army Armament Research, Development and Engineering Center, Armament Engineering Directorate, Picatinny Arsenal, New Jersey.
3. James, H. R.; "Critical Energy Criterion for the Initiation of Explosives by Spherical Projectiles"; Article in Propellants, Explosives, and Pyrotechnics, Vol. 14, 1989, pp. 223–233.
4. Fern, Eric N. and Ramsey, John B.; "Spherical Projectile Impact on Explosives", Paper presented at The Ninth Symposium (International) on Detonation, Aug. 28 – Sept. 1, 1990, Reprints Vol II, pages 662–665.
5. Bahl, K.L., Vantine, H.C., and Weingart, R.C.; "The Shock Initiation of Bare and Covered Explosives by Projectile Impact, " paper in the proceedings of The Seventh Symposium (International) on Detonation, 16–19 June 1981, proceedings published as NSWCMP–82–334. pp. 325–335.
6. Rice, M.H.; "Penetration of High Explosives by Inert Projectiles," SSS–R–78–3512. November 1977, Systems, Science, and Software, P. O. Box 1620 La Jolla, California.
7. Slade, D. C. and Dewey, J.; "High Order Initiation of Two Military Explosives by Projectile Impact," U. S. Army Ballistics Research Laboratory, Aberdeen Proving Ground, MD, Report No. 0121, July 1957.
8. Wilbeck, James S.; "Impact Behavior of Low Strength Projectiles ", Air Force Materials Laboratory Report, AFML–TR–77–134, (1978), Air Force Materials Laboratory, Air Force Wright Aeronautical Laboratories, Air Force Systems Command, Wright–Patterson Air Force Base, Ohio, 45433.
9. Minshall, Stanley F.; "The Dynamic Response of Iron and Iron Alloys to Shock Waves," Response of Metals to High Velocity Deformation, Proceedings of a Technical Conference, July 11–12, 1960, Editors P. G. Shewmon and V. F. Zackay, Interscience Publishers, Inc., New York, pp. 249–274, 1961.
10. Bancroft, D., Peterson, E.L., and Minshall, S.; "Polymorphism of Iron at High Pressures," Journal of Applied Physics, Vol. 27, No. 3, March 1956, pp. 291–298.
11. Held, M.; "Initiierung Von Sprengstoffen., Ein Vielschichtiges Problem Der Detonationsphy Physik", Explosivstoffe, NR.5, 1968, pp. 98–113.
12. Personal Correspondence from Dr. M. Held to J. P. Billingsley, Sept. 6, 1990.
13. Held, M.; "Critical Area for the Initiation of High Explosive Charges," paper in Shock Waves in Condensed Matter – 1983, Ed. by J. P. Asay, R. A. Graham, and G. K. Straub, Elsevier Science Publishers, B. V. 1884. pp. 555–557.
14. Discussion of this topic with Dr. Joe Carlone, Gencorp Aerojet, Azusa, California.

15. Billingsley, J. P. and Oliver, J. M.; "The Relevance of the DeBroglie Relation to the Hugoniot Elastic Unit (HEL) of Shock Loaded Solid Materials." MICOM TR–RD–SS–90–4, (March 1990), Aeroballistics Analysis Branch, Systems Simulation and Development Directorate, U. S. Army Missile Command, Redstone Arsenal, AL, 35898.

16. Rierson, Sean; "Further Analysis and Correlation of Projectile–Target Impact Pressures Including an Elastic Wave Precursor," Article in the 1990 Technical Report of the Science and Engineering Apprentice Program (SEAP), U. S. Army Missile Command, Redstone Arsenal, AL, 35898, pp. 467–474.

17. Barker L. M. and Hollenbach, R. E.; "Shock Study of the $\alpha \Leftrightarrow \varepsilon$ Phase Transition in Iron," Journal of Applied Physics, Vol. 45, No. 11, November 1974, pp. 4872–488.

18. Barker L. M.; "α– Phase Hugoniot of Iron, "Journal of Applied Physics, Vol. 46, No. 6, June 1975, pp. 2544–2547.

19. Green, L. G. Nidick, Jr., E. J., and Walker, F. E.; "Critical Shock Initiation Energy of PBX–9404, A New Approach," Lawrence Livermore Laboratory, University of California, Livermore, Ca. Report UCRL–51522, 25 January 1974.

20 Ramsey, J. B. and Popolato, A.; "Analysis of Shock Wave and Initiation Data for Solid Explosives," Paper presented at The fourth Symposium (International) on Detonation, 12–15 October 1965, published as ACR–126, pp. 233–238, by the Office of Naval Research, Department of the Navy, Arlington, Va.

21. Jameson, J. L., Boyle, V. M., and Sultanoff, M.; "Determination of Shock Hugoniots for Several Condensed Phase Explosives," presented at The fourth Symposium (International) on Detonation, 12–15 October 1965, proceedings published as ACR–126, pp. 241–247, by the office of Naval Research, Department of Navy, Arlington, VA.

APPENDIX
IMPACT SHOCK VARIABLE RELATIONSHIPS AND BASIC DATA

APPENDIX
IMPACT SHOCK VARIABLE RELATIONSHIPS AND BASIC DATA

Iron and some steels, under moderate impact shock loading below 130 Kbars, exhibit a two wave structure where the first one is essentially an elastic wave followed by a slower plastic wave front. The elastic wave is generated under these conditions is called the Hugonoit Elastic Limit (HEL) to distinguish it from a dynamic elastic limit which could occur under less severe loading conditions [9]. The double wave structure requires that computations for pressures and densities be performed via the following equations.

The pressure behind the HEL wave is:

$$P_{HEL} = \rho_o C_L U_{PHEL} \tag{A-1}$$

The density behind the HEL wave is:

$$\varrho_{HEL} = \varrho_o \left(\frac{C_L}{C_L - U_{pHEL}} \right) \tag{A-2}$$

$$\approx \varrho_o \tag{A-3}$$

Equation A-3 is a good aproximation because C_L, the longitudinal wave velocity, is much larger than U_{PHEL} so that $C_L/(C_L - U_{PHEL}) \approx 1.0$. To a good approximation, since U_s, is generally much larger than U_{PHEL}, the shock front pressure corresponding to the paritcle velocity U_P is:

$$P_S = P_{HEL}\ U_S\ (U_P - U_{PHEL}) + P_{HEL} \tag{A-4}$$

Experimentally, it has been found for many materials, that the shock velocity U_S, is a linear function of the particle of velocity, U_P. This relation is commonly represented by:

$$U_S = C_o + S\ U_P \tag{A-5}$$

Where C_0 and S are experimentally determined constants. These constants for iron (or mild steel), PBX-9404, and COMP-B are given in Table A-1. For steel the HEL wave velocity, particle velocity, and pressure values employed were taken from Reference 15. They are:

C_L = 6.04 km/sec
U_{PHEL} = 0.0288 km/sec
P_{HEL} = 13.6 KBARS

In Appendix A of Reference 1, it was shown how to analytically compute the initial contact particle velocities of colliding materials. In Reference 1, the effect of an HEL precursor wave was not considered. However, in Reference 16, the HEL effect was included and this procedure was employed in the present analysis for shock pressures less than or equal to 130 Kbars where a phase transition occurs in the iron or mild steel projectiles. Above P_S = 130 Kbars three waves exist (one elastic and two plastic) until the plastic wave velocity (U_S) exceeds the elastic wave velocity (C_L). This one-wave situation occurs at very high impact velocities (V_I). None of the experimental data analyzed in the present investigation were in this one-wave region, but three data points were in the 3-wave region or very close to it. The initial particle velocities for

these three data points were obtained by the graphical procedure suggested in Reference 1. Table 2 in the main body of this report, contains both the analytical and computed results. Both procedures depend on following expression which is valid at the contact interface of the projectile (P) and explosive (EX).

$$V_I = U_{PP} + U_{PEX} \qquad \text{(A–6)}$$

When the particle velocities are known, then U_S and P_S can be found from the appropriate relations (A–5 and A–4, respectively).

Table A–1
Impact Shocked Material Information

Material ~	ρ_0 Grams/cm^3	C_0 km/sec	S ~	Source ~	Comments ~
Iron or	7.84	4.63	1.33	[17, 18]	$P_S \leq 130$ KBARS
mild steel	7.84	1.10	4.22	[10]	$P_S > 130$ KBARS
PBX–9404	1.84	2.45	2.48	[19, 20]	
Comp–B	1.70	2.95	1.67	[21]	S was modified from 1.58 to 1.67

DISTRIBUTION LIST

	Copies
AMSMI–RD ATTN: Peggy Doran/Mr. Walter Jennings	2
AMSMI–RD–CS–R	15
AMSMI–RD–CS–T	5
AMSMI–GC–IP, Mr. Fred H. Bush	1
U.S. Army Materiel System Analysis Activity ATTN: AMXSY–MP (Herbert Cohen) Aberdeen Proving Ground, MD 21005	1
IIT Research Institute ATTN: GACIAC 10 W. 35th Street Chicago, IL 60616	3
Sandia National Laboratories ATTN: Dr. D. D. Bloomquist P. O. Box 5800 Division 1252 Albuquerque, NM 87185	3
Los Alamos National Laboratory ATTN: Dr. Steven A. Sheffield Group M–9 Mail Stop P–952 Los Alamos, NM 87545	3
Army Research Laboratory Terminal Effects Division AMSMRL–WT–T, Dr. A. Mark Aberdeen Proving Ground, MD 21005–5066	3
Army Research Laboratory Explosive Technology Branch ATTN: AMSMRL–WT–TB, Dr. R. Frey/Dr. V. M. Boyle Aberdeen Proving Ground, MD 21005–5066	3
Los Alamos National Laboratory ATTN: Dr. I. E. Lindstrom Group WX–5 Mail Stop G–780 Box 1663 Los Alamos, NM 87545	3

	Copies
Dr. Thomas J. Ahrens Division of Geological and Planetary Sciences California Institute of Technology Pasedena, CA 91125	3
Baldini Resource Associates, Inc. 10 Barry Lane Newton, NJ 07860	3
Dr. Manfred Held MBB Verteid Igungssysteme Postfach 1340 8898 Schroben Hausen, Germany	3
ATTN: Dr. Ted Nicholas WRDC–MLLN Wright–Patterson AFB, OH 45433	3
Naval Surface Weapons Center ATTN: R12, Dr. J. M. Short White Oak Silver Spring, MD 20903–5000	3
Naval Surface Warfare Center ATTN: Mr. Tom Wasmund / Dr. Bill Holt Code G–13 Dahlgren, VA 22448	3
Eglin Air Force Base ATTN: 46 Test Wing(AFMC), Mr. Bill Dyess Eglin AFB, FL 32542–5000	3
Mr. J. W. Watt 4068 Adams Drive Silver Spring, MD 20902	3
TASC ATTN: Mr. Carl E. Clucus 907 Mar–Walt Drive Fort Walton Beach, FL 32548	2
UAH Reasearch Institute ATTN: Mr. Shane Strickland Mr. Glenn Romanczuk Huntsville, AL 35816	 1 1
Johns Hopkins University ATTN: Professor E. R.Fitzgerald 127 Latrobe Hall 34th and Charles Street Baltimore, MD 21218	3

	Copies
University of Illinois Department of Aeronautical Engineering ATTN: Professor R. A. Strehlow Urbana, IL 61801	3
Army Research Laboratory AMSRL–WT–TD ATTN: Dr. Glenn Randers–Perhson Aberdeen Proving Ground, MD 21005–5066	2
Los Alamos National Laboratory Dr. James P. Richie, Group Leader , Detonation Theory and Applications P. O. Box 1663 M. S. B214 Los Alamos, NM 87545	3
Sandia National Laboratories Dr. Mark B. Boslough Shock Wave and Explosion Physics P. O. Box 5800, Division 1153 Albuquerque, NM 87185	3
Ms. Brigitta Dobratz 543 Todd Loop Los Alamos, NM 87545	2
Dr. W. C. Davis, President Energetic Dynamics 693 4th Street Los Alamos, NM 87545	2
Mr. James Dahm Safety Consulting Engineers, Inc. 5240 Pearl Street Rosemont, IL 60018	2
Sandia National Laboratories ATTN: Dr. G. I. Kerley P. O. Box 5800, Division 1533 Albuquerque, NM 87185	3
Lawrence Livermore National Laboratory ATTN: Dr. M. Van Thiel P. O. Box 808, L–299 Livermore, CA 94550	3
Lawrence Livermore National Laboratory ATTN: Dr. Richard J. Wasley P. O. Box 808, Livermore, CA 94550	3

	Copies
Commander, U. S. ARDEC SMCAR–AEE–W(W) ATTN: Mr. B. Fishburn Picatinny Arsenal, NJ 07806–5000	3
Commander, U. S. ARDEC SMCAR–CCH–V ATTN: Mr. Floyd Hildebrant Picatinny Arsenal, NJ 07806–5000	3
Dr. Michael R. Edwards Royal Military College of Science Department of Mechanical and Civil Engineering Shrivenham, Swindon, Wilts SN68LA, United Kingdom	1
Office of Weapons Safety ATTN: Dr Charles Karnes Science Advisor D. P. 22 U. S. Department of Energy Washington D. C. 20545	3
Sandia National Laboratories ATTN: R. A. Graham P. O. Box 5800, ORG, 1153 Albuquerque, NM 87185	3
Denver Research Institute University of Denver ATTN: Mr. Larry Brown Denver, CO 80208	3
Army Research Laboratory ATTN: Dr. John H. Suckling AMSRL–SL–BF Aberdeen Proving Ground, MD 21005–5066	3
Gencorp Aerojet Dr. Joe Carleone Mr. Roy Iketani Mr. Richard West P. O. Box 296 1100 West Hollyvale Street Azusa, CA 91702	3
Army Research Laboratory ATTN: Dr. T. N. Wright AMSRL–WT–T Aberdeen Proving Ground, MD 21005–5066	3

	Copies
Argonne National Laboratory Technical Information Services Report Unit BLDG. 203 Argonne, IL 60439	3
Department of Mechanical and Aerospace Engineering ATTN: Dr. Yukie Horie North Carolina State University Raleigh, NC 27695	2
Department of Mathematics ATTN: Dr. Julian Wu North Carolina State University Raleigh, NC 27695	2
Director U. S. Army Research Office SLCRO–MS, Dr. Kailasam Iyer Dr. Michael Cistan P. O. Box 12211 Research Triangle Park, NC 27709–2211	2
Los Alamos National Laboratory ATTN: Dr. Jerry Wackerle P. O. Box 1663 Mail Stop P952 Los Alamos, NM 87545	3
Department of Physics ATTN: Dr G. E. Duvall Washington State University Pullman, WA 99164–2814	3
Dr. Y. M. Gupta Shock Dynamics Laboratory Department of Physics Washington State University Pullman, WA 99164–2814	3
Mr. H. C. Rodean Lawrence Livermore National Laboratory Mail Code 262 P. O. Box 808 Livermore, CA 94550	3

	Copies
University of Texas at Austin Dept. of Aerospace Engineering and Engineering Mechanics ATTN: Dr. J. C. Westkaemper Dr. C. H. Yew Dr. E. A. Ripperger W. R. Woolrich Labs Austin, TX 78712–1085	3
Mr. Henry W. Bach SMCCR–MUC Chemical Research, Development, and Engineering Center Aberdeen Proving Ground, MD 21010–5423	3
Dr. M. M. Chaudhri/Dr. J. E. Field Cavendish Laboratory University of Cambridge Madingley Road Cambridge CB30HE England	3
Dr. Henry Eyring Department of Chemistry University of Utah Salt Lake City, UT	3
Dr. Franklin Walker Interplay 18 Shadow Lake Road Danville, CA 94526	2
Dr. James Thoreen Air Force Armament Laboratory AFATL/MN Eglin AFB, FL 32542–5000	3
Dr. Allen J. Tullis IIT Research Institute 10 w. 35th Street Chicago, IL 60616	2
Mr. B. G. Craig 56 Hidden Cove Valparaiso, FL 32580	2
Dr. Phillip M. Howe Los Alamos National Laboratory P. O. Box 1663 ATAC, K574 Los Alamos, NM 875545	3

	Copies
Dr. Michael Cowperswaite SRI International 333 Ravenswood Menlo Park, CA 94025	3
Kaman Sciences Corp. ATTN: Dr. James Wilbeck/Mr. T. S. Pendergrass P. O. Box 2486 Huntsville, AL 35804–2486	3
Dr. Julius Roth Consultant 308 Canyon Drive Portola Valley, CA 94025	2
Dr. Ruth Doherty Naval Surface Warfare Center Bldg. 30, Rm 110 Silver Springs, MD 20904	3
Dr. B. D. Lambourn Atomic Weapons Establishment Aldermaston (AWE) Reading, RG74PR England	3
Dr. Pers – Anders Persson Center for explosive Technology Research Campus Station Socorro, NM 87801	3
Dr. Claude Fauquignon Institute Saint–Louis (ISL) 12, Rue De I'Industrie Saint Lous 68301, France	3
Naval Research Laboratory Dynamics of Solids Branch Condensed Material and Radiation Sciences Division ATTN: Andrew E. Williams Washington, D. C. 20375–2707	3
Rudolph L. Zadnik Potomac Research, Inc. Alexandria, VA 22312–2707	3
Army Research Laboratory AMSRL–SL–B(ATTN:Mr. Ron Hendry) Aberdeen Proving Ground, MD 21005	3

	Copies
Dwight D. Jones/W. B. Thomas Thiokol P. O. Box 400006 Huntsville, AL 35815–1506	3
Dr. M. H. Rice Systems Science and Software P. O. Box 1620 La Jolla, CA 92038	2
Los Alamos National Laboratory ATTN: Dr. J. M. Walsh Dr. R. G. McQueen Dr. S. P. Marsh Dr. J. W. Taylor P. O. Box 1663 Los Alamos, NM 875545	4
Paul A. Urtiew Lawrence Livermore National Laboratory P. O. Box 808, L282 Livermore, CA 94550	1
Craig M. Tarver Lawrence Livermore National Laboratories P. O. Box 808, L282 Livermore, CA 94550	1
LeRoy G. Green Lawrence Livermore National Laboratories P. O. Box 808, L282 Livermore, CA 94550	1
John W. Kury Lawrence Livermore National Laboratories P. O. Box 808, L282 Livermore, CA 94550	1
Edward L. Lee Lawrence Livermore National Laboratories P. O. Box 808, L282 Livermore, CA 94550	1
Donald L. Onellas Lawrence Livermore National Laboratories P. O. Box 808, L282 Livermore, CA 94550	1

	Copies
Arnold Karo Lawrence Livermore National Laboratories P. O. Box 808, L282 Livermore, CA 94550	1
Walter Herrmann P. O. Box 5800, Div. 1500 Albuquerque, NM 87185–5800	1
Dennis B. Hayes P. O. Box 5800, Div. 1530 Albuquerque, NM 87185–5800	1
C. S. Coffey Naval Surface Warfare Center 10901 New Hampshire Ave. Silver Spring, MD 20903–5000	1
Richard Bardo Naval Surface Warfare Center 10901 New Hampshire Ave. Silver Spring, MD 20903–5000	1
Charles Dickinson Naval Surface Warfare Center 10901 New Hampshire Ave. Silver Spring, MD 20903–5000	1
Sigmund J. Jacobs Advanced Technology and Research 1208 Ruppert Road Silver Spring, MD 20903–5000	1
Donna Price Advanced Technology and Research 10901 New Hampshire Ave. Silver Spring, MD 20903–5000	1
John Starkenburg U. S. Army Research Laboratory Aberdeen Proving Ground, MD 21005–5066	1
Richard C. Harrison U. S. Army Research Laboratory Aberdeen Proving Ground, MD 21005	1
Douglas E. Kooker U. S. Army Research Laboratory Aberdeen Proving Ground, MD 21005–5066	1

	Copies
Sam Lambrakos Naval Research Laboratory 4555 Overlook Ave., S.W. Washington, D. C. 20375	1
William E. Deal Los Alamos National Laboratory P. O. Box 1663, MS P915 Los Alamos, NM 875545	1
Charles A. Forest Los Alamos National Laboratory P. O. Box 1663, MS P952 Los Alamos, NM 875545	1
Charles E. Morris Los Alamos National Laboratory P. O. Box 1663, MS J970 Los Alamos, NM 875545	1
Pei Chi Chou Dyna East Corporation 3201 Arch Street Philadelphia, PA 19096	2
Murray Komhauser 3C Systems, Inc. 620 Argyle Rd. Wynnewood, Pa 19096	2
Julius W. Enig Enig Associates, Inc. 11120 New Hampshire Ave. Silver Spring, MD 20904	2
Graeme A. Leiper ICI Explosives Nobels Explosives Co., Ltd. Stevenson, Ayshire, KA20 3LN UK	2
Hugh R. James Atomic Weapons Establishment Foulness Island, Southend on Sea Essex, SS3 9EX UK	2

	Copies
Henry H. P. Moulard Institut Saint–Louis (ISL) 12, Rue De l'Industrie Saint Louis, 68300 France	2
Algot Persson Swedish Detonic Research Foundation Box 32058, S–12611 Stockholm, Sweden	2
Sandia National Laboratories Thermochemical and Physical Division 1534 ATTN: Dr. J. E. Dunn Dr. D. E. Grady Albequerque, NM 87185	2
Sandia National Laboratories Computational Physics and Mechanical Division 1531 ATTN: Dr. J. W. Swegle Albequerque, NM 87185	1
Sandia National Laboratories ATTN: Dr. L. M. Barker Albequerque, NM 87185	1
RAFAEL ATTN: Dr, Y. Partom Dr. Z. Rosenburg P. O. Box 2250 Haifi, 31021, Israel	2
A. Garn Butcher Hercules Inc. P. O. Box 98 Magna, UT 84037	2

		Copies
David Mann U. S. Army Research Office P. O. Box 12211 Research Triangle Park, NC 27709–2211		3
AMSMI–RD–W	Dr. Wharton	3
AMSMI–RD–PR	Dr. Stephens Mr. R. W. Milton	3
AMSMI–RD–WC	Dr. J. S. Bennett Dr. Miles Holloman	3
AMSMI–RD–SS	Dr. Grider Mr. Davis	1 1
AMSMI–RD–SS–SE	Mr. Grabney Mr. Jordan Mr. Waddle	1 1 1
AMSMI–RD–SS–AA	Dr. Billingsley Dr. Oliver Mr. Ward Ms. Crow Ms. Cornelius	10 1 1 1 1
AMSMI–RD–ST–CM	Mr. Parker Mr. Howard	1 1
AMSMI–RD–ST–WF	Mr. Schexnayder Ms. Kraft Mr. Lovelace Mr. Lienau Mr. Hill Mr. Cornelius Mr. MacDonald	1 1 1 1 1 1 1
AMSMI–RD–PR	Dr. O. E. Ayers	1
AMSMI–RD–PR–T	Mr. L. B. Thorn	1
AMSMI–RD–PR–S	Dr. J. S. Murfree	1
AMSMI–RD–PR–M	Mr. Kelly McGuire	1